Thermoeconomical Analysis and Optimization of a Hybrid Solar-Thermal Power Plant Using a Genetic Algorithm

Duarte P. A. Coutinho
duarte.coutinho@tecnico.ulisboa.pt

Instituto Superior Técnico, Universidade de Lisboa, Portugal

January 2021

Abstract

A thermoeconomic model for a small-scale hybrid solar-thermal power plant has been developed to study its performance under different operating conditions. The proposed system consists of a combined Rankine-Brayton cycle with a solar receiver and fossil fuel combustor working in series as heat sources to the topping cycle. An evolutionary algorithm was employed to conduct a multi-objective optimization of such system, and the result was a set of Pareto-optimal designs which were compared to a pre-defined reference design. Resulting optimized designs yield levelized electricity costs as low as 0.179 USD/kWh, as opposed to the 0.237 USD/kWh associated with the reference design. Average 1st and 2nd law efficiencies of up to 27.97 % and 33.53 % were achieved, respectively, which represent increases of up to 7.71 % and 7.31 %. Finally, average solar shares of up to 65 % are possible for optimal designs versus the 58.4 % yielded by the base design.

Keywords: Thermoeconomics, Concentrating Solar Power, Multi-Objective Optimization, Evolutionary Algorithms

1. Introduction

Climate change is among the issues of the century, and one that is already felt at a global scale on the form of increasing average temperatures, natural catastrophes such as droughts and wildfires, melting of the glaciers, etc. At the same time, the demand for fossil fuels as a primary energy source continues to increase, which will inevitably lead to the exhaustion of existent reserves during the upcoming decades. These problems cannot be overlooked and transitioning towards renewable energy sources is mandatory. Solar energy is amongst the most relevant green energy sources, accounting for 8.9 % of the global electricity produced by renewables in 2018, which represents a share of approximately 2.3 % of the global generation [1]. Solar power technologies can be divided into two categories: solar photovoltaic (PV) and concentrating solar power (CSP). One may argue that there is a third category composed of non-concentrating solar-thermal systems such as the flat plate collectors and the evacuated tube collectors, but these options have yet to prove their suitability for electricity generation, thus they will not be discussed here. Historically, the investment in PV systems has been far greater than that of CSP, mainly because this type of technology allows for the direct conversion of solar radiation into electricity, while solar thermal systems convert solar radiation into heat. As a result, PV technologies are more mature and therefore the correspondent levelized electricity cost (LEC) is currently lower, with a global average of 0.068 USD/kWh versus 0.182 USD/kWh for CSP in 2019 [2]. According to IEA, the global electricity generation of solar renewables was 604 TWh in 2018, out of which only 12 TWh (roughly 2 %) account for CSP systems. However, CSP technologies offer some advantages such as a much greater energy storage potential (in the form of heat) with lower associated costs and the possibility for direct integration in an operational power cycle.

Concentrating solar power systems use a set of collectors and/or lenses to reflect incoming solar radiation towards a receiver, where it is converted into heat. This heat can then be transported by a heat transfer fluid - usually a thermal oil - for direct use, production of solar fuels, integration in a power cycle for electricity generation, etc. Currently, there are four distinct commercially established technologies: Parabolic trough collectors (PTC), linear Fresnel reflectors

(LFR), solar power towers (SPT), and parabolic dish collectors (PDC). Parabolic trough collectors are composed of a single long linear focus solar collector with a parabolic shape that concentrates incoming solar radiation into a long receiver tube, heating the heat transfer fluid that flows inside. The collector and solar receiver are fixed to one another and follow the movement of the sun by the action of a single axis sun-tracking mechanism (see figure 1).

PTC systems are the most mature and widely used CSP technology, as well as one of the cheapest. For these reasons, the proposed model employs a PTC setup for solar hybridization. The reader is referred to a book published by Woodhead entitled “CSP technology” [3] for further details on the developments of each technology.

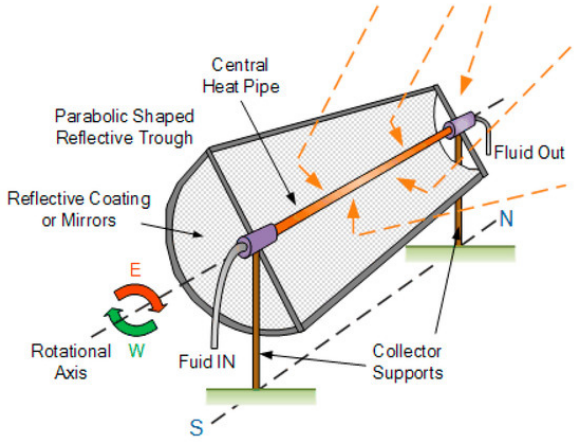

Figure 1 PTC technology [4]

The current work focuses on a hybrid solar-thermal and fossil fuel power plant, an interesting emerging concept. The clear environmental advantages of renewable solar energy coupled with the dispatchability and reliability of fossil fuels delivers a quite versatile power plant, benefiting from the best of both worlds. Continuous generation of electricity during solar downtimes is assured by the combustor, whose short start-up time allows for the system to work with minimal to non-existent thermal storage, reducing costs. Besides, the integration of these hybrids with CO_2 capture technologies such as pre/post combustion sequestration, oxy-fuel combustion or chemical looping combustion as well as the utilization of so called green fuels such as biodiesel are two quite attractive possibilities that could eventually lead to carbon-neutral systems in the future.

2. Modelling

Numerous possible hybrid CSP and fossil fuel configurations have been reviewed and studied by various authors. In their work, Jin and Hong [5] have identified four main categories of existent hybridization approaches: fossil backup and boosting of solar thermal power plants; solar-aided coal-fired power plants; integrated solar combined cycle (ISCC) plants; and advanced systems. The current work focuses on a model idealized in a previous master thesis (see Rodrigues [6]) that falls into the last category. It consists of a Brayton-Rankine combined cycle with a solar receiver and a combustor working in series as heat sources to the topping cycle. It proposes the addition of a regenerator after the compressor that recovers part of the heat discharged by the gas turbine (see figure 2). The heat exchanger (HEX) and condenser are responsible for discharging heat from the system, and water at 15 ºC and 1 bar is chosen as the cold fluid for both. The model assumes that this water is captured from a nearby river, and thus its cost is neglected. Pressure drops were defined in accordance with the works of Dunham and Lipinski [7] and Rodrigues [6]: 5 % inside the solar

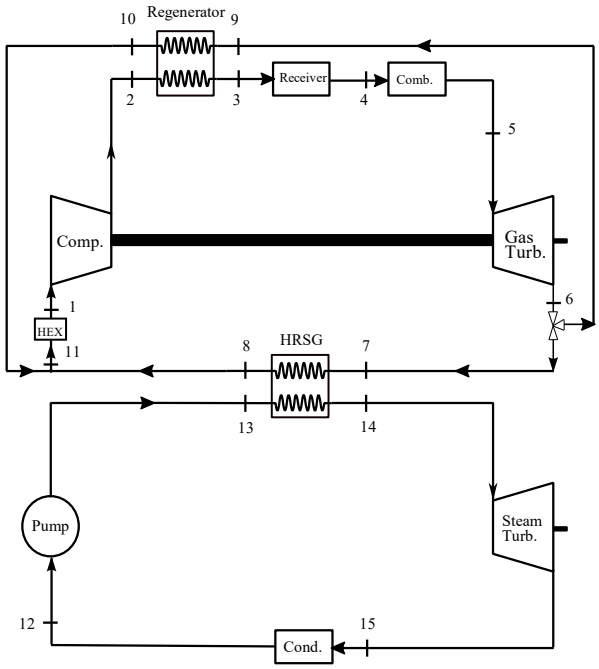

Figure 2 Proposed model [6]

receiver, an estimation based on the work of Pye [8], and 2 % for each heat exchanger as well as the combustor. Loss of pressure inside the transmission pipes is neglected. The minimum temperature and pressure are set to $T_1 = 308\ K$ and $p_1 = 1\ bar$.

At the bottoming cycle, the working fluids temperature at the pump inlet, T_{12}, is fixed to 308 K, and its pressure, p_{12}, is either the saturation or ambient pressure, whichever is greater, assuring that it is either in saturated liquid or compressed liquid phase. At the pump outlet, the fluid's pressure is set to the value between p_{12} and 20 bar that yields the highest net power for the Rankine cycle, considering the imposed thermodynamic restrictions.

A total of 25 fluid combinations were initially considered for the system: CO_2, Air, N_2, He and H_2 for the topping cycle and Water, Toluene (C_7H_8), Cyclopentane (C_5H_{10}), Octamethyltrisiloxane ($C_8H_{24}O_2Si_3$) and Hexamethyldisilane ($C_6H_{18}OSi_2$) for the bottoming cycle. A preliminary analysis conducted under fixed standard conditions evidenced CO_2 and Cyclopentane as the fluid pair with the best thermodynamic performance, so it was chosen for the optimization analysis.

The thermoeconomic model of the system was developed and simulated using a MatLab® algorithm that was developed for that matter. It can be divided in two parts: the first is responsible for computing the energy streams flowing through each component and it is similar to Rodrigues's program [6]. The second part calculates the flows of exergy and the system costs, which is completely new with regard to Rodrigues's work [6]. The ability to run the simulations under different ambient conditions was also added to the program. It starts off by setting specific thermodynamic properties to key points (or states) of the system. Most of these properties are inherent to the model itself and were previously described, while others are user-defined inputs, which are summarized in table 1. It then goes on calculating additional properties for each state by means of the mass and energy balances of each component (equations (1) and (2)) coupled with thermodynamic computational software. For this purpose, the program employs polynomial functions presented in the work of McBride et al. [9] for calculations referring to the topping cycle, and the C++ library of thermodynamic properties CoolProp for calculations referring to the bottoming cycle.

Table 1 MatLab® program inputs

Input variable	Symbol
Nominal solar flux = DNI	$G_0\ [W/m^2]$
Ambient temperature	$T_{amb}\ [K]$
Compression ratio	$p_r = p_2/p_1$
Mass flow ratio	$r = \dot{m}_9/\dot{m}_1$
Gas turbine inlet temperature	$T_5\ [K]$
Regenerator heat transfer area	$A_{reg}\ [m^2]$
Steam turbine inlet temperature	$T_{14}\ [K]$
Solar collector area	$A_{col}\ [m^2]$
Compressor isentropic efficiency	η_{comp} [%]
Gas turbine's isentropic efficiency	η_{GT} [%]
Steam turbine isentropic efficiency	η_{ST} [%]
Pump isentropic efficiency	$\boldsymbol{\eta_{pump}}$ [%]

Once all the thermodynamic states and energy streams are fully defined, the program employs entropy and exergy balances (equations (3) and (4)) to compute the specific exergy at each state as well as the exergy destruction inside each component.

$$\iint \rho\, \vec{V} \cdot \vec{n}\, dA = 0 \tag{1}$$

$$\dot{Q} - \dot{W} = \iint h\rho\, \vec{V} \cdot \vec{n}\, dA \tag{2}$$

$$\iint \left(\frac{\dot{Q}}{T}\right)_b dA + \dot{\sigma} = \iint s\rho\, \vec{V} \cdot \vec{n}\, dA \tag{3}$$

$$\iint \dot{Q}\left(1 - \frac{T_0}{T_b}\right) dA - \dot{W} - \dot{E}_{x_d} = \iint e_{x_f} \rho\, \vec{V} \cdot \vec{n}\, dA \tag{4}$$

$\rho - Specific\ mass$

$\vec{V} - Velocity$

$\dot{Q} - Rate\ of\ energy\ exchange\ in\ the\ form\ of\ heat$

$\dot{W} - Rate\ of\ energy/exergy\ exchange\ in\ the\ form\ of\ work$

$\dot{\sigma} - Rate\ of\ entropy\ generation$

$s - Specific\ entropy$

$T_0/T_b - Ambient/heat\ transfer\ boundary\ temperatures$

$\dot{E}_{x_d} - Rate\ of\ exergy\ destruction$

$e_{x_f} - Specific\ flow\ exergy$

Then, the thermodynamic feasibility of the simulated solution is checked by a routine that applies a set of restrictions, and all unfeasible solutions are discarded. Finally, the costing model is applied to define system costs related to operation and maintenance, fuel usage, land acquisition, component's purchase, etc. Statistical correlations, which are present in the literature [10–14], were used to approximate the capital investment in component's acquisition.

The chosen location for the generation unit was Évora, Portugal (38.57º N, 7.91º W), given the high insolation values of this southern region. Typical values for the direct normal irradiance (DNI) and ambient temperature of the site were taken from a typical meteorological year (TMY) data file, available in EnergyPlus™ database. The model was simulated for the following days, representative of each season: 10th of January (Winter), 23rd of March (Spring), 28th of June (Summer) and 5th of October (Fall).

3. Multi-Objective Optimization

A multi-objective optimization (MOO) was conducted in order to find the Pareto-optimal designs of the given system. For this matter, an evolutionary algorithm denominated "gamultiobj" was employed. It is a computational routine available in MatLab's optimization toolbox, and a variant of the state-of-the-art NSGA-II controlled elitist genetic algorithm. The developed algorithm and the "gamultiobj" MOO tool interact with each other as illustrated in figure 3.

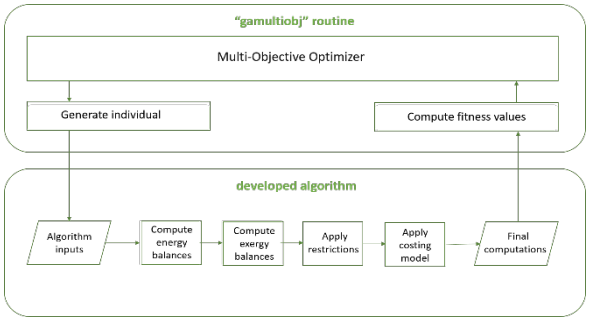

Figure 3 Algorithm flowchart and interaction with the MOO routine

3.1. Preliminary analysis

Initially, the developed algorithm was used independently to define a reference design for comparison with the optimized designs. For this matter, most input variables were fixed to certain values of interest, while a set of iterative compression ratios (p_r) and mass flow ratios (r) were considered as follows.

1) $p_r \in [1 : 0.1 : 20]$
2) $r \in [0.01 : 0.01 : 0.99]$
3) $T_5 = 825\ \mathrm{K}$
4) $A_{reg} = 6\ m^2$
5) $T_{14} = 550\ \mathrm{K}$
6) $A_{col} = 200\ m^2$
7) $\eta_{comp} = 79.6\ \%$
8) $\eta_{GT} = 85.8\ \%$
9) $\eta_{ST} = 68.0\ \%$
10) $\eta_{pump} = 60.0\ \%$

Results of these preliminary simulations are presented on table 2. The algorithm was developed in such a way that the 1st law efficiency is directly constrained by the user-defined gas turbine inlet temperature (T_5) and compression ratio (p_r), so in the colder months were the gas temperature at the receiver's outlet is lower, the system will compensate by burning more fuel in order to achieve the desired T_5. This is the reason why η_{global} does not change seasonally. On the other hand, exergetic efficiency peaks during Summer due to a higher ambient temperature, while the net power output peaks during Winter. The behaviour of this last property is also

Table 2 Results of the preliminary simulations – reference/base design

Season	**Summer**		**Fall**		**Winter**		**Spring**	
Maximization objetive	**Max. η & ε**	**Max. $\dot{W}_{net}$**	**Max. η & ε**	**Max. $\dot{W}_{net}$**	**Max. η & ε**	**Max. $\dot{W}_{net}$**	**Max. η & ε**	**Max. $\dot{W}_{net}$**
p_r	6.6	6.6	6.6	6.6	6.6	6.6	6.6	6.6
r	0.01	0.33	0.01	0.34	0.01	0.36	0.01	0.34
η_{global} [%]	20.26	19.08	20.26	19.00	20.26	18.81	20.26	18.98
ε_{global} [%]	26.22	23.85	25.70	23.21	24.71	22.00	25.22	22.75
$\dot{W}_{net}$ [kW]	31.32	32.59	31.74	33.54	33.80	36.82	33.30	35.49
$\dot{E}_{x_{d,system}}$[kW]	81.15	96.61	82.54	100.76	86.68	111.33	84.77	104.71
$\dot{Q}_{input}$ [kW]	154.62	170.83	156.68	176.48	166.85	195.67	164.37	186.98
f_{sol} [%]	62.95 %	56.97 %	59.55 %	52.87 %	53.70 %	45.79 %	57.51 %	50.56 %

explained by the functioning of the algorithm: a colder day results in a lower solar receiver outlet temperature, T_4, which in turn results in higher mass flow ratios of the topping and bottoming cycle fluids and consequently higher power outputs. This analysis revealed that for the given set of input variables, the system's maximum 1st and 2nd law efficiencies were achieved for a mass flow ratio of 0.01, the minimum considered value, while the system's maximum work output was achieved for mass flow ratios between 0.33 and 0.36, depending on the season. Additionally, the $r = 0.01$ scenario is the most profitable, as it yields the maximum net present value (NPV), and the maximum work output scenario is not profitable at all, yielding a negative NPV. This was the first indication that the valve and regenerator might be dispensable, depending on the system's objective. Consequently, the MOO analysis was applied not only to the initially proposed model (with regenerator), but also to the same model without regenerator or stream splitting valve in order to compare the performance of both designs. The maximum efficiencies scenario was considered as the reference/base design, as it is the most profitable one, so the considered compression ratio and mass flow ratio were 6.6 and 0.01, respectively.

3.2. Objective functions

The main targets of the MOO were to maximize the system's thermodynamic performance, increasing revenue, while minimizing associated costs. Therefore, total investment cost (C_{inv}) minimization and net present value (NPV) maximization were chosen as the objective functions. To calculate the investment cost, eq. (5) was employed, which considers three contributions: costs associated with equipment purchase (C_{eqp}); land acquisition (C_{land}); and power electronics, construction & civil engineering (C_{civil}). This approach was based on the methodology used by Pihl et al. [11]. The direct capital cost of purchase of each equipment was approximated by costing equations available in the literature as function of their main thermodynamic parameters. Statistical correlations presented in the works of Bejan et al. [10], Pihl et al. [11], Guo-Yan et al. [12] and El-Sayed [13] were used for that matter, and the resultant values were converted into 2019 dollars using the chemical engineering plant cost index (CEPCI). The land purchase and civil engineering related costs were estimated based on simplifying correlations proposed by Turchi [14].

$$C_{inv} = C_{eqp} + C_{land} + C_{civil}\ [€] \qquad (5)$$

For the calculation of the net present value, equation (6) was employed,

$$NPV = -C_{inv} + \sum_{t=1}^{n} \frac{R - C_{O\&M}}{(1+i)^t}\ [€] \qquad (6)$$

where R stands for the yearly revenue of the power plant and $C_{O\&M}$ is the yearly operation and maintenance costs, which were divided into two categories – equipment associated costs ($C_{o\&m_{eqp}}$) and fuel cost ($C_{o\&m_{fuel}}$) - and were calculated as follows:

$$C_{o\&m_{eqp}} = C_{eqp} \cdot f \cdot (\varphi - 1)\ [€/y] \qquad (7)$$

$$C_{o\&m_{fuel}} = \dot{m}_{fuel} \cdot C_{fuel} \cdot LHV_{fuel} \cdot H\ [€/y] \qquad (8)$$

In equation (7), the maintenance factor (φ) was assumed to be 1.06, and the annuity factor (f) was calculated for an interest rate of 8 % and a power plant lifetime of 25 years. In equation (8), $\dot{m}_{fuel}$ and C_{fuel} represent the mass flow (in kg/s) and specific cost (in €/kWh) of the natural gas burnt in the combustor, respectively. The parameter H accounts for the yearly operating time of the system and was assumed to be 4015 [h/y] according to the number of solar hours throughout the year. The specific cost of natural gas was assumed to follow an increasing trend of 0.3 % (average inflation in Portugal, 2019) for each year of operation, taking on the initial value of 40.1 €/MWh (average cost of N.G. for industrial users in 2019, accounting for all service expenses such as transmission, distribution, etc.). These two values were taken from rigorous statistics published by PORDATA on their webpage [15]. The yearly revenue (R) was computed under the assumption that the system would supply a small community, working as an auto-consumption unit that may or may not be connected to the main grid. Therefore, it was calculated as the savings that such a community would sustain if all its electricity came free of charge directly from the system instead of the main grid, as exposed in eq.

(9). The increasing trend on the specific cost of electricity ($C_{electricity}$) was also assumed to be 0.3 % for each year of operation, taking on the initial value of 215 €/MWh (average cost of electricity for domestic users in 2019, accounting for all service expenses such as transmission, distribution, etc. [15]). The computation of the electrical power output, $\dot{P}_{el}$, was based on the net work output and considered a typical electrical generator efficiency of 96 %.

$$R = C_{electricity} \cdot \dot{P}_{el} \cdot H \ [€/y] \quad (9)$$

3.3. Decision variables

The program inputs exhibited on table 1 were considered as decision variables, with the exception of those that determine the ambient conditions, G_0 and T_{amb}, which assumed fixed yearly average values during the MOO ($G_0 = 646.7\ \mathrm{W/m^2}$ and $T_{amb} = 18.08\ ºC$). Logically, when analyzing the model without regenerator, only 8 optimization variables were considered, excluding the mass flow ratio and regenerator area. For each decision variable, the following ranges of values were considered:

1) $p_r \in [1,20]$
2) $r \in [0.01,0.99]$
3) $T_5 \in [800\ \mathrm{K}, 900\ \mathrm{K}]$
4) $A_{reg} \in [2\ m^2, 10\ m^2]$
5) $T_{14} \in [500\ \mathrm{K}, 575\ \mathrm{K}]$
6) $A_{col} \in [200\ m^2, 400\ m^2]$
7) $\eta_{comp} \in [75\ \%, 90\ \%]$
8) $\eta_{GT} \in [75\ \%, 90\ \%]$
9) $\eta_{ST} \in [60\ \%, 75\ \%]$
10) $\eta_{pump} \in [60\ \%, 75\ \%]$

3.4. Performance indicators

For each Pareto-optimal solution, the algorithm computes a set of performance indicators to be used as references for the measurement of its performance. The global cycle's 1st (η_{global}) and 2nd law efficiencies (ε_{global}), electrical power output ($\dot{P}_{el}$), and total heat input ($\dot{Q}_{input}$) quantify the thermodynamic performance of the system, while the payback period (PBP), the internal rate of return (IRR) and the levelized electricity cost (LEC) quantify the economic performance of the system. The calculation of the PBP is straightforward and requires no explanation, the IRR is computed using a MatLab® function, and the LEC is calculated in a simplifying manner as follows:

$$LEC = \frac{f \cdot C_{inv} + C_{o\&m}}{\dot{P}_{el} \cdot H} \ [€/kWh] \quad (10)$$

Finally, the solar share (f_{sol}), mass of CO_2 emissions and savings ($m_{CO_2\ emitted}$ and $m_{CO_2\ saved}$) quantify the environmental performance of the system. The carbon dioxide emissions savings correspond to the additional mass of CO_2 that would be released into the atmosphere if the same system was entirely powered by the combustion chamber. These performance indicators are calculated as follows:

$$f_{sol} = \frac{Q_s}{Q_s + Q_c} [\%] \quad (11)$$

$$m_{CO_2\ emitted} = \dot{m}_{fuel} \cdot \frac{M_{CO_2}}{M_{CH_4}} \ [kg/s] \quad (12)$$

$$m_{CO_2\ saved} = \frac{f_{sol} \cdot m_{CO_2\ emitted}}{1 - f_{sol}} \ [kg/s] \quad (13)$$

where Q_s and Q_c are the heat inputs to the system through the solar receiver and combustion chamber, respectively. In equation (12), M_{CO_2} and M_{CH_4} stand for the molecular weights of carbon dioxide and methane, respectively. This equation assumes stoichiometric combustion of the fuel, which is considered to be methane (CH_4) as an approximation

3.5. Results and discussion

The results of the MOOs were a pair of Pareto fronts composed of 70 subjects each, as illustrated on fig. 4.

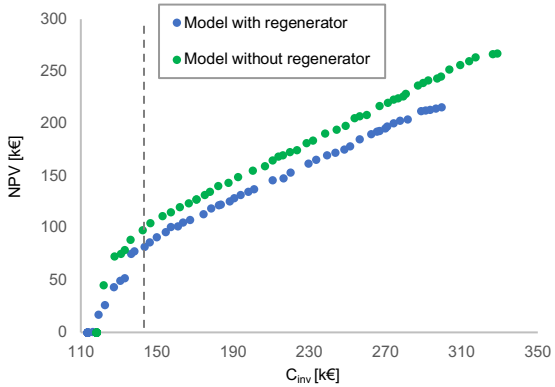

Figure 4 Resultant Pareto fronts

Looking at the two Pareto fronts, it is possible to conclude that the results from the MOO of the model without regenerator dominate those of the model with regenerator throughout most of the considered domain, with the exception of the very low NPV subjects, which are not very interesting

from the economical perspective. This is a strong evidence that the system's thermoeconomical performance is indeed stronger if the regenerator is eliminated. The truth is that without this component the model's exergy destruction is decreased, and a larger amount of heat is transferred to the bottoming cycle, increasing its power output. Additionally, with the elimination of the regenerator it is possible to have a greater solar collector area as well as more efficient components for the same investment cost. Therefore, the further analysis refers to the no regenerator model, which was considered to be a more interesting design.

The Pareto front is made up of Pareto-optimal designs which assume a wide range of values for the decision variables (genes) - as illustrated in fig. 5 - and performance indicators. It can be divided in two distinct regions: the first region, composed of the first 27 subjects, where the local derivative of the plot keeps changing $(f'(i) = (NPV_i - NPV_{i-1})/(C_{inv_i} - C_{inv_{i-1}}))$, and the second region, composed of the last 43 subjects, where such derivative assumes a more steady close to unit value. The transition between regions is marked with a dashed line in figures 4 and 6-8.

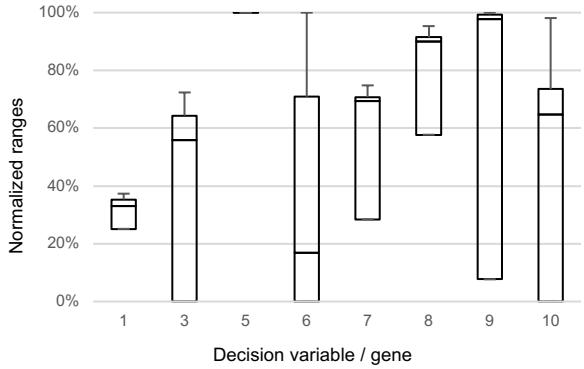

Figure 5 Genetic distribution of Pareto-optimal solutions based on the previously defined ranges

The NPV increases with C_{inv} throughout the Pareto front, thus a higher initial investment results in a higher profit in the future. The fitness values of Pareto-optimal solutions go from investment costs of 118,264 € with near zero NPV values, to 328,706 € worth of investment for a net present value of 267,373 €. Similar conclusions can be drawn from the payback period and levelized electricity cost, which decrease with C_{inv}(see figure 6), and the internal rate of return, which increases with C_{inv}. Optimal solutions boast levelized electricity costs on the order of 0.159 – 0.221 €/kWh, which corresponds to 0.179 – 0.248 USD/kWh according to the considered conversion rate. These results show that the optimized system can yield similar or lower costs of electricity generation than conventional stand-alone CSP systems, which take on global average LEC values of 0.182 USD/kWh according to IRENA [2]. However, from a strictly economic point of view, it clearly falls behind when compared to standard natural gas fired combined cycle power plants, whose LEC typically falls on the 0.041 – 0.074 USD/kWh range according to Lazard's data [16].

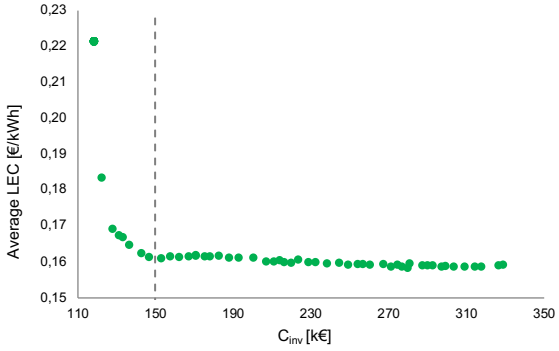

Figure 6 Levelized electricity costs of Pareto-optimal solutions

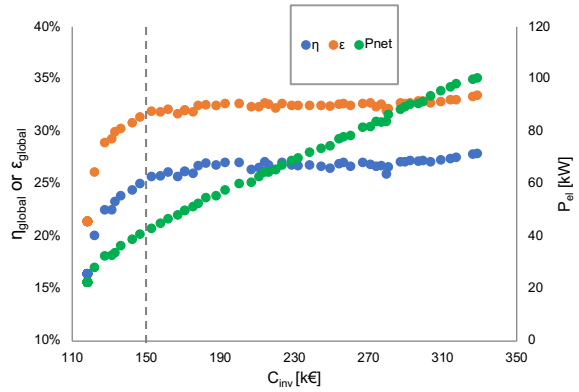

Figure 7 Global 1st and 2nd law efficiencies and electrical power outputs of Pareto-optimal solutions

Both efficiencies (1st and 2nd law) follow an increasing trend along the first region, and then begin to stabilize after the transition to the second region at around 26.9 % and 32.6 %, respectively. These values, which fall within the range of 16.46 % – 27.97 % and 21.49 % – 33.53 %, represent a valuable improvement comparing to the base case design, which boasts maximum 1st and 2nd law efficiencies of 20.26 % and 26.22 % respectively (see table 2). On the other hand, the system's net electrical power output increases almost linearly throughout both regions. This proves that the second is the optimal efficiency

region, where the main variation from one subject to another is the increase of the collector field area accompanied by an increase on the system's size and power output (economy of scale), as illustrated in figure 7.

The solar share (f_{sol}) is the highest for the first subject (~ 65 %), and then assumes a decreasing trend until the 36th subject, where it stabilizes at around 51 % (see figure 8). This behaviour is highly related to the evolution of p_r and T_5, which also stabilize at the 36th subject, as well as A_{col}, whose growth rate stabilizes at the same point. Furthermore, the employed algorithm invalidates any solution with a solar share under 50 %, so this is the minimum acceptable value. As a reference, if we look at the Pareto-optimal solution with the closest NPV to that of the base case (13,420 €) and compare the solar shares of both solutions, we see that the optimized design yields an average solar share of almost 65 %, which represents an increase of roughly 6.5 % on an annual average basis, for an investment that is 20 % lower. These results reveal the clear superiority of the optimized designs from an environmental point of view. Since the system's power output and input are increasing with investment cost, it is expected that the annual mass of CO_2 emissions saved due to the hybridization also increase with C_{inv}, even though the same trend does not apply to the solar share (see figure 8). For a design with the maximum considered solar collector's area of 400 m^2, the amount of CO_2 that is not discharged to the environment due to the impact of the solar hybridization is over 150 tons per year.

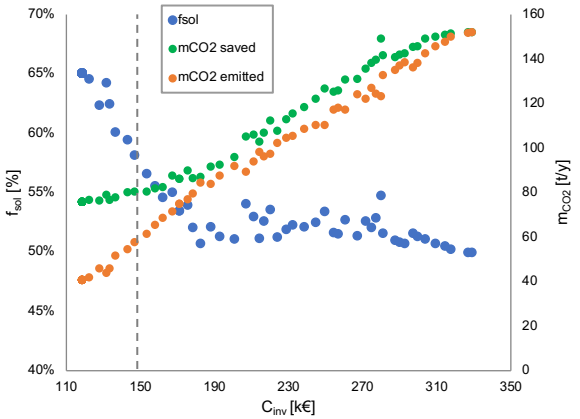

Figure 8 Environmental performance indicators of Pareto-optimal solutions

It is important to point out that all of the 70 subjects are optimal solutions, in a sense that it is impossible to improve one of the objective functions without hurting the other, thus it is the designer's task to consider all the solutions and chose the one(s) that better fit the purpose of the system. With this in mind, three distinct decision-making scenarios were idealized, resulting in three different optimized designs. The first scenario consists of a solution based on economic criteria and represents an interesting choice for an investor who is focused on financial return. The second focuses on thermodynamic criteria and idealizes a suitable option for an investor whose decision making is highly constrained by funds and available land, and whose objective is to maximize generation power ($\dot{P}_{el}$). Finally, the third emphasizes environmental criteria and prioritizes a greener solution. Figure 9 and table 3 summarize the most important results of each scenario. These parameters have been normalized in fig. 9 to facilitate comparison, and the thermodynamic indicators, which change seasonally, have been averaged over the four representative days.

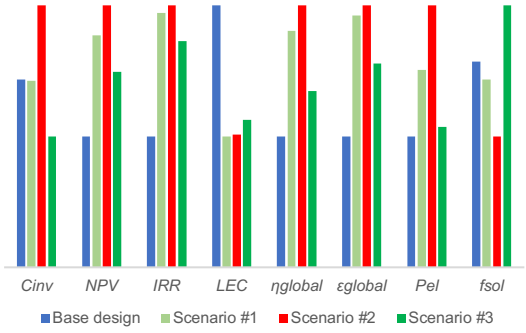

Figure 9 Comparison of different scenarios regarding normalized fitness values and performance indicators of interest

The chosen design for the first scenario yields a NPV of 111,585 €, which comparing to the base design represents an increase of 98,165 € (731.5 %), for an initial investment that is 0.2 % lower (152,858 €). Furthermore, the project becomes profitable after 7 years, which is 3 years earlier than the base design, the IRR is 6.66 % higher and the LEC assumes the competitive value of 0.161 €/kWh. Even with a significantly higher power output, the total exergy destruction of the system remains virtually unchanged. The biggest downside of this solution is the lower solar share (1.83 % reduction on an annual average basis) and consequential higher CO_2 emissions (annual average increase of 14.01 %) comparing to the base case.

For the second scenario, the resultant investment cost is almost 19 % higher (182,221 €), but the NPV and generated power are also much greater, with respective percentual

Table 3 Genes, fitness values and performance indicators of interest of Pareto-optimal solutions

		Optimized designs		
	Base design	***Scenario #1 (Economic criteria)***	***Scenario #2 (Thermodynamic criteria)***	***Scenario # (Environmental criteria)***
Decision variables / Genes				
p_r	6.6	6.58	7.97	6.44
r	0.01		X	
T_5 $[K]$	825	843.72	867.04	802.44
A_{reg} $[m^2]$	6		X	
T_{14} $[K]$	550	575	575	575
A_{col} $[m^2]$	200	211.78	229.36	208.04
η_{comp} [%]	79.6	85.34	85.39	83.64
η_{GT} [%]	85.8	88.53	88.72	87.98
η_{ST} [%]	68	74.66	74.88	74.47
η_{pump} [%]	60	67.56	70.05	63.12
Objective functions / Fitness values				
C_{inv} [€]	153,192.7	152,858.1	182,221	131,102.5
NPV [€]	13,420.4	111,584.9	140,483.9	75,690.7
Performance indicators				
PBP [y]	10	7	7	7
IRR [%]	8.99	15.66	16.06	14.14
LEC [€/kWh]	0.211	0.161	0.162	0.168
η_{global} [%] *	20.26	25.76	27.08	22.63
ε_{global} [%] *	25.46	32.04	32.61	29.42
$\dot{P}_{el}$ [kW] *	31.24	43.40	55.16	33.00
$\dot{Q}_{input}$ [kW] *	160.63	175.53	212.18	151.91
$\dot{E}_{x_{d,system}}$[kW] *	83.79	83.68	103.52	72.51
f_{sol} [%] *	58.43	56.60	50.73	64.25
$\dot{m}_{co_2\ emitted}$ [kg/h] *	13.53	15.42	21.17	11.01
$\dot{m}_{co_2\ saved}$ [kg/h] *	18.93	20.05	21.71	19.70

*Annual average basis

increases of 946.8 % (140,484 €) and 76.6 % (55.16 kW) on an annual average basis. The economic performance of this design is generally good, but the system exergy destruction rate is 23.55% greater (on an annual average basis) than that of the base case. This is due to the higher scale of the system, with its remarkably higher compression ratio, component isentropic efficiencies, gas turbine temperature inlet, and solar collector area, which also explains the much greater electrical power output. At the same time, it assumes a quite poor environmental performance, with solar shares as low as 46.5 % and CO_2 emissions as high as 23.88 kg/h during Winter, representing deviations from the base case of -7.2 % and +53 %, respectively.

Finally, the third scenario is the only one that outperforms the base design in every considered parameter. The net present value of 75,691 €, representing an increase of 464 %, is achieved for a lower investment cost of 131,103 € (-14.4 %). The gas turbine inlet temperature is minimized, greatly reducing the mass of burnt fuel and thus achieving solar shares of up to 69 % in Summer. A reduction of 20.4 % in CO_2 emissions is achieved for this season, evidencing the superior environmental performance of the design. Lower heat generation inside the combustor is compensated by a larger area of solar collectors, as well as higher steam turbine inlet temperature and component isentropic efficiencies, ultimately resulting in an even higher electrical power output. Globally, the system exergy destruction rate is reduced by 13.46 % on an annual average basis.

4. Conclusions

A thermoeconomical model for a hybrid solar-thermal power plant was developed in a MatLab®

environment and used to conduct a multi-objective optimization of the system. Results demonstrate the potential for the integration of CSP technology in natural-gas-fired combined cycle microgeneration units.

The MOO revealed that there is a great opportunity for improvement of the system's thermodynamic, economic, and environmental performance by eliminating the regenerator from the model and varying certain operating parameters. The resultant Pareto front is composed of 70 optimal subjects. During the decision-making process, three of these designs were selected, each of them corresponding to the most suitable solution for three different scenarios which focus on economic, thermodynamic and environmental performance, respectively.

References

[1] IEA, "World Energy Outlook 2019", 2019. https://www.iea.org/reports/world-energy-outlook-2019 (accessed November 3, 2020).

[2] IRENA, "Solar Energy" (n.d.). https://www.irena.org/solar (accessed June 24, 2020).

[3] K. Lovegrove, W. Stein, *"Concentrating solar power technology*", WoodHead Publishing Ltd., 2012.

[4] H. Olia, M. Torabi, M. Bahiraei, M.H. Ahmadi, M. Goodarzi, M.R. Safaei, "Application of nanofluids in thermal performance enhancement of parabolic trough solar collector: State-of-the-art", Appl. Sci. 9 (2019).

[5] H. G. Jin, H. Hong, "Hybridization of concentrating solar power (CSP) with fossil fuel power plants", in: *Concentrating Solar Power Technology - Principles, Developments and Applications*, Woodhead publishing, 2012, ch. 12, pp. 395–420.

[6] J.A.M. Rodrigues, "Hybrid Solar Thermal Power Plants", Msc. thesis, Dept. Mech. Eng., Instituto Superior Técnico, Lisbon, Portugal, 2019.

[7] M.T. Dunham, W. Lipiński, "Thermodynamic analyses of single Brayton and combined Brayton-Rankine cycles for distributed solar thermal power generation", J. Sol. Energy Eng. Trans. ASME. 135 (2013).

[8] J. Pye, G. Morrison, M. Behnia, "Pressure drops for direct steam generation in line-focus solar thermal systems", Aust. New Zeal. Sol. Energy Soc. Conf. (2006).

[9] B. J. McBride, M. J. Zehe, S. Gordon, "NASA Glenn coefficients for calculating thermodynamic properties of individual species", Glenn Research Center, Cleveland OH, USA, NASA/TP—2002-211556, Sep. 2002.

[10] A. Bejan, G. Tsatsaronis, M. Moran, "Thermal Design and Optimization", John Wiley & Sons , 1996.

[11] E. Pihl, J. Spelling, F. Johnsson, "Thermo-economic optimization of hybridization options for solar retrofitting of combined-cycle power plants", J. Sol. Energy Eng. Trans. ASME. 136 (2014) 1–9.

[12] Z. Guo-Yan, W. En, T. Shan-Tung, "Techno-economic study on compact heat exchangers", Int. J. Energy Res. 32 (2008) 1119–1127.

[13] Y.M. El-Sayed, "Designing desalination systems for higher productivity", Desalination. 134 (2001) 129–158.

[14] C. Turchi, "Parabolic Trough Reference Plant for Cost Modeling with the Solar Advisor Model (SAM)", National Renewable Energy Laboratory (NREL), Golden CO, USA, NREL/TP-550-47605, July 2010.

[15] PORDATA, "Base de Dados Portugal Contemporâneo", (n.d.). https://www.pordata.pt (accessed July 3, 2020).

[16] Lazard, "Levelized Cost of Energy and Levelized Cost of Storage - 2020". "https://www.lazard.com/perspective/levelized-cost-of-energy-and-levelized-cost-of-storage-2020/" (accessed October 24, 2020).